GLIA

GLIA 58:1437–1450 (2010)

Oligodendrocyte Precursors Originate in the Parabasal Band of the Basal Plate in Prosomere 1 and Migrate into the Alar Prosencephalon During Chick Development

RAQUEL GARCIA-LOPEZ AND SALVADOR MARTINEZ*
Developmental Biology Unit, Instituto de Neurociencias, UMH-CSIC, Alicante, Spain

KEY WORDS
myelin precursors; diencephalon development; cell migration; brain regionalization

ABSTRACT
Oligodendrocytes are the myelin-forming cells in the central nervous system of vertebrates. Oligodendrocyte precursors arise from multiple restricted foci distributed along the antero-posterior axis of the developing brain. In chick and mouse embryos, oligodendrocyte precursors of the anterior forebrain emerge from neuroepithelial cells of the subpallium and migrate tangentially to invade the entire telencephalon (Olivier et al. (2001) Development 128:1757–1769). In the diencephalon, oligodendrocyte neuroepithelial precursors seem to be mainly located in the basal plate of caudal prosomeres, but very little is known about their distribution and maturation at later stages of embryonic development. Thus, in this work, we studied the origin and migration of oligodendrocyte precursos in the diencephalon of quail-chick chimeras. Homotopic and homochronic grafts demonstrated that, during embryonic development, diencephalic oligodendrocytes emerge from a common neuroepithelial domain in the basal plate of prosomere 1 and migrate tangentially, invading the dorsal regions of the diencephalic prosomeres and the telencephalon.

INTRODUCTION

Oligodendrocytes are myelin-forming cells in the vertebrate central nervous system (CNS) (Asou et al., 1995; Kettenmann and Ransom, 1995). During embryonic development, their precursors arise from proliferating cells located in small regions distributed throughout the ventricular epithelium (Noll and Miller, 1993; Olivier et al., 2001; Perez-Villegas et al., 1999; Small et al., 1987; Warf et al., 1991). In these regions, oligodendrocyte precursors can be identified by the expression of *PDGFR*α (Hall et al., 1996; Pringle and Richardson, 1993) or *plp/dm-20* (Delaunay et al., 2008; Spassky et al., 1998; Timsit et al., 1995). PDGFRα is a tyrosine kinase receptor implicated in a variety of developmental processes, including the proliferation and survival of oligodendrocyte precursor cells (OPC) (Noble et al., 1988; Richardson et al., 1997; Soriano, 1997). *Plp/dm-20* belongs to the dm family of genes whose members have been identified in the shark, ray (Kitagawa et al., 1993), and mouse (Yan et al., 1993). *Plp* encodes two alternatively spliced products: the proteolipid protein (PLP) and DM-20, which are proteins with four putative transmembrane domains (Popot et al., 1991; Wahle and Stoffel, 1998) and are the main proteic components of myelin in the CNS of higher vertebrates (Griffiths et al., 1998; Lees and Brostoff, 1984). Although *plp* is expressed during the final stages of oligodendrocyte maturation, its corresponding transcript can be detected much earlier during embryonic development (Timsit et al., 1992). Indeed, the presence of restricted subsets of *plp/dm20+* neuroepithelial cells in the mouse embryonic brain and spinal cord suggests a link between *plp* expression and early oligodendrogenesis (Delaunay et al., 2008; Dickinson et al., 1996; Timsit et al., 1995).

The origin of oligodendrocytes has mainly been studied in the spinal cord. Here, OPCs are generated in the ventricular zone of the basal plate, just dorsal to the floor plate (Nishiyama et al., 1996; Ono et al., 1995; Orentas and Miller, 1996; Pringle and Richardson, 1993; Pringle et al., 1992, 1996; Timsit et al., 1995; Warf et al., 1991; Yu et al., 1994). In the chick spinal cord, O4-positive preoligodendrocytes migrate radially, populating the basal mantle layer, and ventrodorsally toward the alar mantle layer, where they mature to form myelin (Miller and Ono, 1998; Ono et al., 1995). In addition to this local migration, retroviral-labeling experiments demonstrated that OPCs also migrate tangentially for over 300 μm along the anteroposterior axis of the spinal cord (Leber and Sanes, 1995; Leber et al., 1996).

In the brain, homotopic and homochronic quail-chick chimeras have demonstrated that OPCs emerge from the medial subpallium and entopeduncular areas, where they migrate tangentially to colonize the entire telencephalon (Olivier et al., 2001). Similar results have been detected in mammals using specific molecular markers [reviewed by Spassky et al. (2000) and Ono et al. (2009)]. OPC migration has been mainly studied in the optic nerve (Cochard and Giess, 1995; Noll and Miller,

Grant sponsor: European Union; Grant number: U.E. LSHG-CT-2004-512003 EUREXPRESS; Grant Sponsor: European Leukodystrophy Foundation (ELA Foundation); Grant Sponsor: Research Spanish grant; Grant number: BFU2008-0058; Grant Sponsor: CIBERSAM; Grant number: CB07/09/0021; Grant Sponsor: INGENIO 2010 MEC-CONSOLIDER; Grant number: CSD2007-0002.

*Correspondence to: Salvador Martinez, Instituto de Neurociencias, UMH-CSIC, Universidad Miguel Hernandez, Campus de San Juan, C/ Ramon y Cajal sn, E-03550, San Juan de Alicante, Spain. E-mail: smartinez@umh.es

Received 3 February 2010; Accepted 22 April 2010

DOI 10.1002/glia.21019

Published online 26 May 2010 in Wiley InterScience (www.interscience.wiley.com).

1993; Ono et al., 1997), where fluorochrome-labeling experiments in chick embryos demonstrated that a subpopulation of oligodendrocytes originate in the ventricular neuroepithelium of the third ventricle (Ono et al., 1997). In the rhombencephalon, the origin and distribution of the oligodendrocytes seem to be restricted to the rhombomeric segments (Perez-Villegas et al., 1999).

The segmental organization of the diencephalon was experimentally demonstrated using quail-chick chimeras (Garcia-Lopez et al., 2004), in agreement with the brain-segmentation paradigm (Puelles and Rubenstein, 2003; Puelles et al., 2007). Three diencephalic segments were described: pretectum (p1), thalamus (p2), and prethalamus (p3) (Fig. 1a). These diencephalic prosomeres, similar to the rhombomeres of the hindbrain and spinal cord, present the four longitudinal histogenetic domains of the neural tube: floor, basal, alar (ap), and roof plates (García-López et al., 2004).

The expression pattern of OPC markers in the diencephalic neuroepithelium suggests that oligodendroglial lineage is specified in a longitudinal domain at the lateral edge of the basal plate, known as the parabasal band (pb) (Delaunay et al., 2008, 2009; Garcia-Lopez et al., 2009; Gimeno and Martinez, 2007; Ono et al., 2008) (Fig. 1b). The discontinuous and heterogeneous expression of these markers suggests that there are segmental-related differences in the OPC generation. Nevertheless, changes in molecular expression throughout development may induce erroneous anatomical interpretations based on the supposedly clonal relationships between ventricular OPC and mature oligodendrocytes. Therefore, to experimentally elucidate the origin and migration of OPC in the diencephalon, we created avian neural chimeras (Alvarado-Mallart and Sotelo, 1984; LeDouarin, 1969, 1993). Using this model, we first identified the ventricular foci of oligodendrogenesis in the diencephalon, and, afterward, we analyzed OPC migration pattern during embryogenesis.

Homotopic and homochronic transplants of diencephalic *plp/dm-20+* neuroepithelium in the parabasal regions demonstrated that, during embryogenesis, the OPC, as well as GABAergic neurons, mainly originate in the parabasal neuroepithelial domains of the caudal diencephalon (prosomere p1) and migrate extensively toward diencephalic and telencephalic alar plates.

Abbreviations

3V	third ventricle
ap	alar plate
APT	anterior pretectal nucleus
APTD	anterior pretectal nucleus, dorsal part
APTp	anterior pretectal nucleus, superficial cell plate
APTs	anterior pretectal nucleus, superficial plexiform layer
APTV	anterior pretectal nucleus, ventral part
b	basal band
ca	anterior commissure
Cb	cerebellum
CoP	commissural pretectum
cpv	compact periventricular stratum
dap	dorsal alar plate
DLA	dorsolateral anterior nucleus of the thalamus
DMA	dorsomedial anterior nucleus of the thalamus
DPT	diffuse pretectal area
flm	fasciculus longitudinal medial
fp	floor plate
fr	fasciculus retroflexus
Hb	habenular nucleus
HPO	hypothalamic periventricular organ
Hy	hypothalamus
ICl	intercalated nucleus
ICo	intercollicular area
IGL	intergeniculate leaflet
III	oculomotor nucleus
InC	interstitial nucleus of Cajal
InR	rostral interstitial nucleus
IPT	intermediate pretectal nucleus
Is	isthmus
lfb	lateral forebrain bundle
lraq	lateral recess of the aqueduct
Mes	mesencephalon
MG	avian medial geniculate nucleus
mtg	mammillo tegmental ttract
opt	optic tract
oq	optic chiasm
os	optic stalk
OT	optic tectum
p1	prosomere 1
p1MT	p1 medial terminal nucleus
p1SNC	p1 substantia nigra, compact part
p1Tg	p1 tegmentum
p1VTA	p1 ventral tegmental area
p2	prosomere 2
p2Tg	p2 tegmentum
p2VTA	p2 ventral tegmental area
p3	prosomere 3
pb	parabasal band
pc	posterior commissure
PcP	precommissural pretectum
Pe	periventricular stratum
PG	pregeniculate nucleus
pm	paramedian band
POA	preoptic area
PRot	perirotundic area
PrPT	principal pretectal nucleus of the commissural pretectum
PT	pretectum
PTh	prethalamus
PThE	prethalamic eminence
PV	posteroventral nucleus of the thalamus
RM	retromammillary area
Rot	rotundus nucleus
rp	roof plate
Rt	reticular nucleus
RtD	reticular nucleus, dorsal part
RtV	reticular nucleus, ventral part
SAC	stratum album centrale of the tectum
SCH	suprachiasmatic nucleus
SGC	stratum griseum centrale of the tectum
SGFS	stratum griseum et fibrosum superficiale of the tectum
sm	stria medullaris
SPC	superficial parvicellular nucleus of the thalamus
SpL	lateral spiriformneuropil
SpM	medial spiriform nucleus
SPT	subpretectal nucleus
SRot	subrotundus nucleus of the thalamus
STh	subthalamic nucleus
SubG	subgeniculate nucleus of the prethalamus
Tect	optic tectum
TEL	telencephalon
TGS	tectal gray, superficial stratum
Th	thalamus
ToS	torus semilunaris
tst	tecto-spinal tract
tt	tectothalamic tract
v	ventricle
Va	ophthalmic nerve
vap	ventral alar plate
Vg	trigeminal ganglia
ZLI	zona limitans intrathalamica

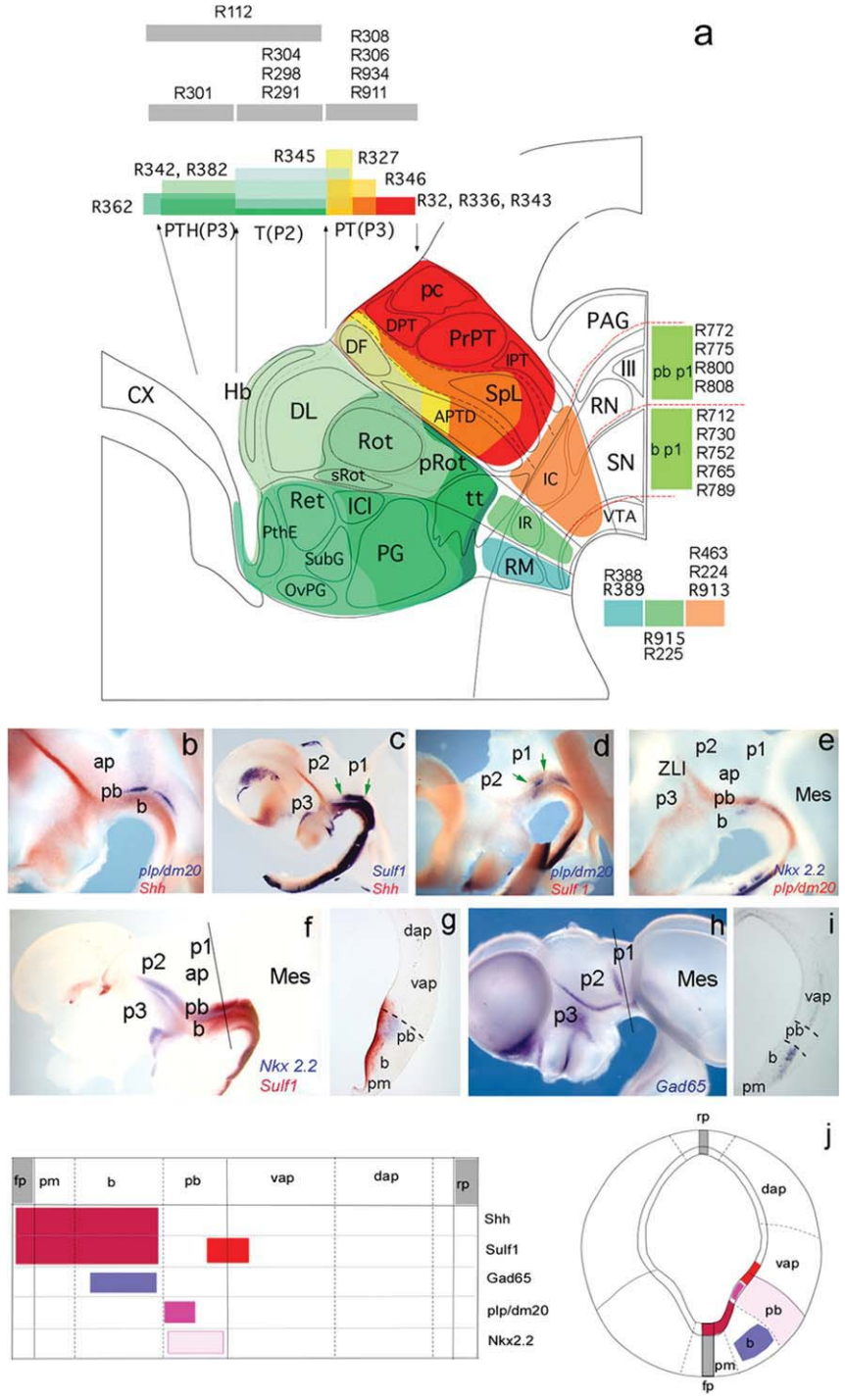

Fig. 1. Diencephalon fate map and gene expression patterns. (**a**) Schematic representation that summarizes the fate mapping analysis and graft position. The colored areas indicate the territories derived from previously performed grafts (Garcia-Lopez et al., 2004), in a hypothetic sagittal section of chick embryo at stage HH35. The top part of the drawing (gray bars) indicates the new grafts performed for this report. (**b–i**) *In situ* hybridization of whole-mount chick embryos at stage HH25 for *plp/dm20*, *Nkx2.2*, *Shh*, *Sulf1*, and *Gad65*. In all images, the neural tube is placed laterally, and rostral is left, dorsal is up. (b) Double *in situ* hybridization for *plp/dm20* and *Shh* expression. (c) Topography of *Sulf1* and *Shh* expression patterns. Arrows indicate the extension of *Sulf1* expression in the parabasal column in p1. (d) Double *in situ* hybridization for *plp/dm20* and *Sulf1* genes. Arrows indicate the extension of *Sulf1* expression in the parabasal column in p1. (e) Double *in situ* hybridization for *Nkx2.2* and *plp/dm20*. (f) Double *in situ* hybridization for *Nkx2.2* and *Sulf1* expression. The line indicates the section plane shown in (g). (g) Coronal section through prosomere 1 of the sample shown in (f). The dashed line marks alar-basal limit. (h) *In situ* hybridization of *Gad65*. The line indicates the section plane shown in (i). (i) Coronal section of the embryo shown in (h) at the p1 level. The dashed line marks the limit of the parabasal column. (**j**) Schematic representation that summarizes the expression pattern of several genes (indicated by different colors) in the basal and parabasal plates, both in a planar representation (left is the ventral midline and right is the dorsal midline) and a coronal section of prosomere 1 at stage HH25. For abbreviations, see abbreviation list.

MATERIALS AND METHODS

Fertilized chick (*Gallus gallus*) and quail (*Coturnix coturnix japonica*) eggs from commercial sources were incubated horizontally at 37°C in a forced air incubator. The stages of the embryos were established according to Hamburger and Hamilton (1951) for the chick and by neural tube morphology for the quail embryos to graft equivalent stages of development.

In Situ Hybridization in Whole-Mount Embryos

Antisense digoxigenin-labeled riboprobes for *Sulf1*, *Shh*, *Nkx2.2*, *Gad65*, and *plp-dm20* were synthesized and subsequently processed for *in situ* hybridization as previously described by Henrique and collaborators (1995). Several whole-mount embryos were processed for double-stained hybridization using digoxigenin (dig)- and fluorescein (f)-labeled antisense riboprobes. The digoxigenin-labeled probes were stained in dark blue using an NBT/BCIP solution, whereas the fluorescein-labeled probes were stained in red, using an INT/BCIP solution, using a standard protocol. After hybridization, embryos were washed in PBT [phosphate-buffered saline solution (PBS) with 0.1% Tween 20], photographed under a dissecting microscope (Leica), and stored at 4°C in PBT/0.1% sodium azide.

Quail-Chick Chimeras

Homotopic and homochronic quail-chick grafts were performed using quail embryos as donors. Quail and chick eggs from commercial sources were used. To perform the surgical procedure at the same stage, the quail eggs were placed in the incubator 3–4 h after the chick eggs, due to their faster rate of development. The chimeras were performed at stage HH9–10 and fixed at different developmental stages.

Microsurgery

The experiments were performed under sterile conditions. The host and donor's shells were partially opened to prepare the embryos for the grafting procedure. The embryos were counterstained *in vivo* with Indian ink, diluted 1:1 in Tyrode's solution supplemented with antibiotics (penicillin 1,000 UI/mL, streptomycin 10 mg/mL) (Gibco, Invitrogen Corporation) and injected under the blastoderm using a glass micropipette. Chick embryos at stage HH9 and the equivalent stage in quail embryos were selected for neuroepithelial grafts. The vitelline membrane that covers the embryo was slipped out of the egg with a tungsten needle at the level of the anterior embryonic region where the microsurgery was to be performed. A grid with concentric circles was inserted in one ocular of the operating microscope to normalize the graft dimensions between different experiments, thus controlling the proportions and topography of the explant/implant neuroepithelium in the donor and host embryos, respectively. The selection of the grafted area in each experiment was performed according to our diencephalic fate map (García-López et al., 2004). At the working magnification used during microsurgery (×40), the radial distance increment between the concentric circles in the grid measured 40 μm. This grid was positioned in relation to the embryo: the vertical axis followed the embryo's ventral midline, the transversal axis was positioned by crossing the optic-diencephalic angle bilaterally, and the anterior pole of the embryo was localized at the anterior frame at 360–400 μm of the central reference point. The selected fragment was excised from the host embryo, and the references with the ocular frame were annotated. An equivalent piece of tissue from the quail donor was transferred to the chick egg using a glass micropipette. The piece of neural tissue was inserted into the groove left after the excision, preserving the original rostrocaudal and dorsoventral orientation. We grafted the ap and basal plate of diencephalic prosomeres 1–3.

When the grafting operation was complete, the opening in the eggshell was sealed with a piece of Scotch tape and incubated in a horizontal stable position until the stage selected for fixation. The chimeras were sacrificed at different stages of development. All the described cases in this work fulfilled the strictest criteria of an adequate development of the chimeric brain, with regards to the graft integration into the host, and with the absence of morphological anomalies. A total of 34 embryos were selected for this study; of these, 17 chimeric embryos were fixed at stages HH24–26 (short survival experiments) to study the time course and pathways of the tangentially migrating cells; nine chimeric embryos were fixed at a more advanced stage (HH29–HH33) to study the neuroepithelial origin and distribution of the migrating cells; and eight chimeric embryos were fixed at stages HH38–40 (long survival experiments) to study the phenotype of the migrating cells.

Analysis of the Chimeras

Short-survival specimens were fixed at stages HH24–29 (4.5–6 days of incubation) by overnight immersion of the embryo's head in 4% paraformaldehyde in PBS (0.1 M, pH 7.4). Afterward, the neural tube was isolated and rinsed in PBT (PBS with 0.1% Tween 20), dehydrated using increasing concentrations of methanol, and stored in 100% methanol at −20°C before being processed for immunostaining and for *in situ* hybridization. Whole-mount immunostaining was performed to detect quail tissues using a monoclonal antiquail antibody (QCPN, Developmental Hybridoma Bank, IowaCity, IA). In several experiments, we additionally processed the brain by *in situ* hybridization using RNA probes (Henrique et al., 1995) to detect *Shh* and *Sulf1* transcripts before processing for immunohistochemistry. Digoxigenin-labeled RNA probes were prepared from plasmids kindly provided by J. Rubenstein (*Shh*) and C. Soula (*Sulf1*). RNA-labeled

probes were detected by an alkaline-phosphatase-coupled antibody (Roche Diagnostics, Mannheim, Germany), and NBT/BCIP was used as a coloring substrate for the alkaline phosphatase staining (Boehringer, Mannheim, Germany). After hybridization, embryos were washed in PBT.

Long-survival chimeras were fixed at HH35–43 stages (9–17 days of incubation) by overnight immersion of the embryo's head in Clarke's fixative or 4% paraformaldehyde in PBS.

The heads fixed in Clarke's were progressively dehydrated in ethanol and processed by paraffin embedding. Twelve micrometer-thick serial sections were cut in horizontal, sagittal, or coronal planes and mounted in several parallel series. One section series was stained with cresyl violet, whereas the other series were processed for single or double immunohistochemistry as described below.

We performed double immunohistochemistry stainings combining QCPN-Mab and specific cellular markers: PLP-monoclonal antibody (specific oligodendrocyte marker; a kind gift from B. Zalc, Paris), Tuj1 (specific neuronal body and axonal marker; Developmental studies Hybridoma Bank, Iowa), and Map2 (specific neuronal body and dendrite marker, Chemicon). For double immunostaining, QCPN-Mab (a nuclear marker) was used as the primary antibody, using a biotinylated secondary antibody and the standard avidin–biotin–diaminobenzidine (DAB) visualization procedure (Vector Laboratories, Burlingame, CA). Bound peroxidase was stained using 0.05% DAB, 0.025% nickel–ammonium sulfate, and 0.01% hydrogen peroxide, in PBS (0.1 M, pH7.4), obtaining a black-colored staining. The sections were rinsed and then incubated in the primary antibodies of the cell markers commented previously. This reaction was also stained with the standard avidin–biotin–DAB procedure; however, in this case, the bound peroxidase was not stained with nickel–ammonium sulphate (thus maintaining the brown color from the DAB and hydrogen peroxide reaction).

In several select experiments, the embryo was fixed in 4% paraformaldehyde and processed for *in situ* hybridization using RNA probes (Henrique et al., 1995) to detect *plp/dm20* and *Gad65* transcripts before processing for immunohistochemistry. Chick embryos were fixed by overnight immersion of the embryo's head in 4% paraformaldehyde in PBS (0.1 M, pH 7.4). All brains were extracted, postfixed for 48 h at 4°C, embedded in 4% agarose, and sectioned transversally in 100-μm-thick slices with a vibratome (Leica). RNA-labeled probes were detected by an alkaline-phosphatase-coupled antibody (Roche Diagnostics, Mannheim, Germany), and NBT/BCIP was used as a chromogenic substrate for the alkaline phosphatase (Boehringer, Mannheim, Germany). After hybridization, the sections were washed in PBT and processed for immunohistochemistry to detect quail cells using the monoclonal QCPN.

Neural Tube Dissection and Organ Tissue Culture

To make the organ tissue culture, we used the protocol previously described by Echevarria and collaborators (2001). Heads from E5 (HH226) embryos were cut at the level of rhombomeres (r) 4–5. Thereafter, the neural tube was opened along the dorsal midline (roof plate) by cutting open the tube caudal-rostrally. Explant tissue was transferred to sterile Petri dishes and placed (ventricular part facing up) on floating polycarbonate membrane filters with 10% fetal bovine serum in DMEM culture medium (Gibco-Life Technologies). Glutamax (2 mM; Gibco-Life Technologies) and penicillin–streptomycin (100 U/mL–100 μg/mL; Gibco-Life Technologies) were added to the culture medium.

DiI Labeling

We used a lipophilic fluorescent carbocyanine dye: 1-1V-dioctadecyl-3,3,3V,3V-tetramethylindocarbocyanine perchlorate (DiI). The DiI crystal was implanted in the neural tube at level of the basal plate of prosomere 1. Explants were generally maintained for up to 24 h in an incubator at 37°C, with 5% CO_2, and 95% humidity. After 24 h of culture, explants were fixed in 4% formaldehyde in PBS. All procedures were carried out under sterile conditions.

RESULTS

Identification of OPC-Generating Neuroepithelial Domains in the Diencephalon

We analyzed 34 embryonic chimeras with homotopic grafts of alar or basal neuroepithelium. The transplants were performed at stage HH9 and fixed at different stages of development. Chimeras fixed at early stages of development (HH24–26) were processed by whole-mount analysis, paraffin-embedded, and sectioned (Figs. 1 and 2). The transplanted regions were detected by QCPN and compared with the expression of *Shh*, *plp/dm20*, and *Sulf1* detected by *in situ* hybridization. *Plp/dm20* and *Sulf1* expressions in the parabasal region of the basal plate are considered to be indicators of oligodendroglial specification (Braquart-Varnier et al., 2004; García-López et al., 2009; Perez-Villegas et al., 1999) (Fig. 1b–g). Two different regions in the neuroepithelium of the diencephalic basal plate were detected: *Shh* was expressed in the whole basal plate (Fig. 1b,c), whereas *Sulf1* was extended to the parabasal column (Fig. 1f,g) (Garcia-Lopez et al., 2009).

We grafted p2 ap in five embryonic chimeras and p2 basal plate in two embryonic chimeras (Figs. 1a and 2a–h). Cases R291 and R915 are, respectively, examples of these grafts (Figs. 1a and 2a–h; Table 1). In R291, the grafted region developed into thalamic ap, dorsal to *Shh* expression (Fig. 2a–d). Analyzing transversal sections of this case, we observed *Shh* expression in the basal plate neuroepithelium of p2 while quail tissue was detected in the dorsal band of the alar plate (dap) (Fig. 2b–d). R915, as previously commented, is a representative basal plate graft (Fig. 1a), where we also mapped the expression pattern of *Sulf1* (Fig. 2e–h). Transversal sections clearly

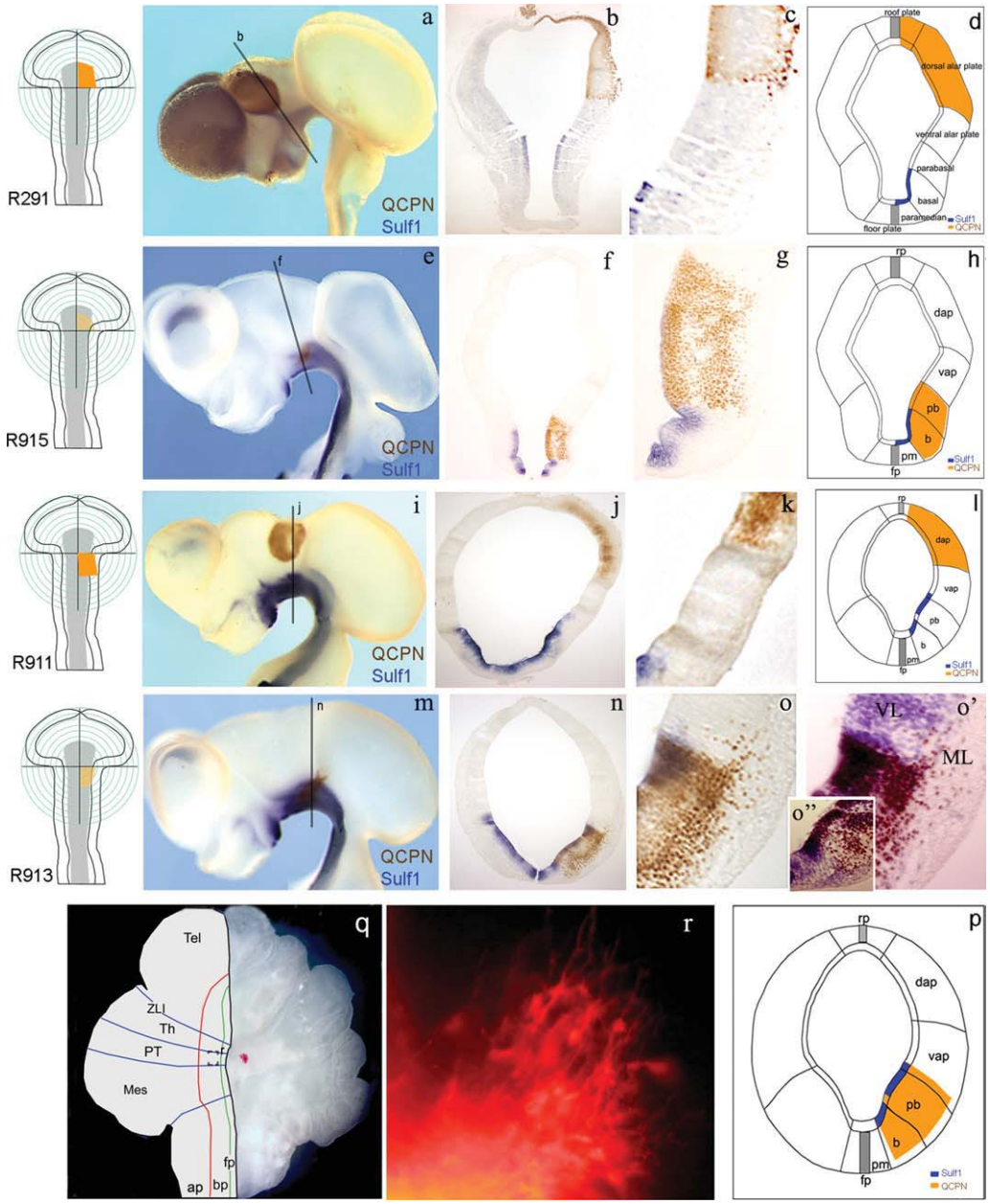

Fig. 2. Analysis of alar and basal-plate quail-chick chimera grafts at short survival times (Table 1). (**a–d**) Represents the results after thalamus graft. (a) HH26 neural tube where the quail transplant was detected by whole-mount immunostaining against quail cells (QCPN) and processed by *in situ* hybridization for *Shh*. The scheme at the left side represents the transplanted epithelium. The line marks the plane of sections shown in (b–c). (b, c) Low and high-power magnifications of a p1 transverse section of the case shown in (a). *Shh* expression indicates the basal-plate neuroepithelium. Quail derivatives are detected in the alar plate. (d) Schematic representation of the section showing the grafted territory (orange) and *Shh* expression in the ventricular epithelium of the basal plate (blue). (**e–h**) Experimental embryo with a basal p2 graft. (e) HH25 whole-mount chick embryo where the quail transplant was detected by QCPN, double stained with *Sulf1* by *in situ* hybridization. The scheme at the left side represents the transplanted epithelium (shaded area indicates the basal-plate territory). The line marks the plane of sections shown in (f–h). (f–h) Low-powered (f) and high-powered (g) images of a coronal section. (h) Representative schematic of the same embryo showing the grafted territory in the p1 basal plate (brown) and *Shh* expression in the ventricular epithelium of the basal plate (blue). (**i–l**) Chimeric neural tube with a pretectal graft (alar p1). The scheme at the left side represents the transplanted epithelium. (i) Whole-mount neural tube at HH25 where the quail transplant was detected by QCPN antibody and *Sulf1* expressing cells were revealed by *in situ* hybridization. The line represents the plane of sections shown in (j, k). (j–l) Coronal sections and interpretative drawing of the same embryo, showing the grafted territory (brown/orange) and *Sulf1* expression in the basal plate (blue). (**m–p**) Results after basal prosomere 1 grafts. The scheme at the left side represents the transplanted epithelium and the line represents the plane of sections shown in (n–p). (m) Picture from a whole-mount chick embryo (HH25) where the quail transplant was detected by QCPN. Basal plate and parabasal band were detected by *in situ* hybridization for *Sulf1*. (n–p) Coronal sections and schematic representation of the same embryo depicting the grafted territory (brown) and *Sulf1* in the basal plate (blue). The section shown in (o) was counterstained with Nissl's stain in (o′) and (o″) to better recognize the cellular zones in the neural wall. (**q**, **r**) Organotypic explants of chick embryo neural tube (q) and high-powered microphotograph showing dorsally migrating cells from the DiI microcrystal inserted in parabasal p1. For abbreviations, see abbreviation list. [Color figure can be viewed in the online issue, which is available at www.interscience.wiley.com.]

TABLE 1. List of Short-Survival Chimeric Embryos Where the Graft Was Implanted in the Dorsoventral Axis of the Neural Tube

Cases	Graft location	Stage of operation	Stage of fixation	Section type	Section plane	Immunohistochemistry/*in situ* hybridization
R308	APp1	HH10	HH24	Paraffin	Coronal	*QCPN*
R306	APp1	HH10	HH25	Paraffin	Coronal	*QCPN*/*Wnt8b*
R934	APp1	HH9	HH24	Paraffin	Coronal	*QCPN*/*Gbx2*
R911	APp1	HH9	HH25	Paraffin	Coronal	*QCPN*/*Sulf1*
R304	APp2	HH10	HH24	Paraffin	Coronal	*QCPN*/*Shh*
R298	APp2	HH10	HH24	Paraffin	Coronal	*QCPN*/*Shh*
R230	APp2	HH9	HH24	Paraffin	Coronal	*QCPN*/*Gbx2*
R291	APp2	HH9	HH25	Paraffin	Coronal	*QCPN*/*Shh*
R301	APp3	HH9	HH24	Paraffin	Coronal	*QCPN*
R112	APp2/p3	HH9	HH26	Paraffin	Coronal	*QCPN*/*Shh*
R913	BPp1	HH8	HH24	Paraffin	Coronal	*QCPN*/*Sulf1*
R463	BPp1	HH9	HH23	Paraffin	Coronal	*QCPN*
R224	BPp1	HH9	HH24	Paraffin	Coronal	*QCPN*
R915	BPp2	HH9	HH24	Paraffin	Coronal	*QCPN*/*Sulf1*
R225	BPp2	HH9	HH24	Paraffin	Coronal	*QCPN*
R389	BPp3	HH9	HH24	Paraffin	Coronal	*QCPN*
R388	BPp3	HH8	HH24	Paraffin	Coronal	*QCPN*

Note: In the graft location column: APp1, p2, p3: alar plate prosomere 1, prosomere 2, prosomere 3; BPp1, p2, p3: basal plate prosomere1, prosomere 2, prosomere3. HH, stages of Hamburger and Hamilton (1951); QCPN, monoclonal antiquail antibody.

TABLE 2. List of Chimeric Embryos Selected to Study the Neuroepithelial Origin of the Tangentially Migrating Cells Within the PBp1

Cases	Graft location	Stage of operation	Stage of fixation	Section plane	Cytoarchitecture (CV) and immunohistochemistry
R712	b p1	HH9	HH29	Coronal	CV, QCPN
R730	b p1	HH9	HH28	Coronal	CV, QCPN, CB
R752	b p1	HH9	HH29	Coronal	CV, QCPN, CB
R765	b p1	HH9	HH30	Coronal	CV, QCPN
R789	b p1	HH9	HH29	Coronal	CV, QCPN, CB
R772	pb p1	HH9	HH29	Coronal	CV, QCPN, CB
R775	pb p1	HH9	HH30	Coronal	CV, QCPN, CB
R800	pb p1	HH9	HH28	Coronal	CV, QCPN, CB
R808	pb p1	HH9	HH29	Coronal	CV, QCPN

Note: In the graft location column: b p1: basal band of basal plate prosomere 1, pb p1: parabasal band of basal plate prosomere 1. CB, anti-calbindin polyclonal antibody; CV, cresyl-violet Nissl stain; HH, stages of Hamburger and Hamilton (1951); QCPN, monoclonal antiquail antibody.

showed that the quail tissue derived toward the basal (b) and pb of p2-basal plate (Fig. 2f–h). We did not detect any cellular movements outside of p2-grafted cellular clusters, neither in the epithelial nor in the mantle layers of the corresponding neural tube wall.

Prosomere 1 ap and basal plate were transplanted into 16 embryos (Tables 1 and 2; Figs. 1a and 2i–p). Four chimeras with alar plate grafts were processed at short survival times (HH25, 4.5 days of incubation) to map the distribution of the donor tissue. The grafted tissue, as seen in embryo R911, developed dorsally to the expression pattern of *Sulf1* (Fig. 2i–l). Conversely, R913 is a representative example of a p1 basal-plate graft, in which we also detected the expression of *Sulf1* (Fig. 2m–p and Table 1). Quail cells were detected in all p1 basal plates when transversal sections of this chimera were analyzed, both in basal and pbs (Fig. 2n–p). In addition, quail cells were found migrating in the mantle layer and, from the basal plate, moved toward the neighboring territories of the alar plate (Fig. 2o). Quail-migratory cells were less numerous in subventricular regions and were never observed in the marginal zone (Fig. 2n–p). We did not detect quail-cell movements in other regions (anterior, posterior, or ventral graft-host boundaries), suggesting that the migration exclusively follows a ventrodorsal direction.

To analyze if this migration also occurs in a nonchimeric experiment, brain neuroepithelium (from rhombencephalon to prosencephalon) was isolated from HH26 embryos (5 days of incubation) and mounted on polycarbonate membranes ($n = 15$). Afterward, a DiI microcrystal was inserted in the basal plate of p1, and the neural tube was cultured for 24 h. Dispersed DiI-labeled cells with the typical migratory morphology (elongated body with clear training and leading processes) were detected moving from the crystal (basal plate) to the alar plate (Fig. 2q,r; $n = 12$). Confirming the previous results from chimeras, we did not detect significant cell movements toward rostral or caudal directions.

We also performed grafts of the alar ($n = 10$) and basal ($n = 5$) mesencephalon that were processed to explore cellular migrations to the pretectum, discarding significant cellular movements in alar territories. Nevertheless, some scattered cells migrated from basal mesencephalon into p1 (data not shown).

Tangential Migration of OPC from p1 pb

Once we detected, these cellular movements in the p1 basal plate, we decided to search for the precise origin of these cells by grafting different dorsal and basal domains of diencephalic segments and analyze them at later stages of development: HH28–43 (6–18 days of incubation).

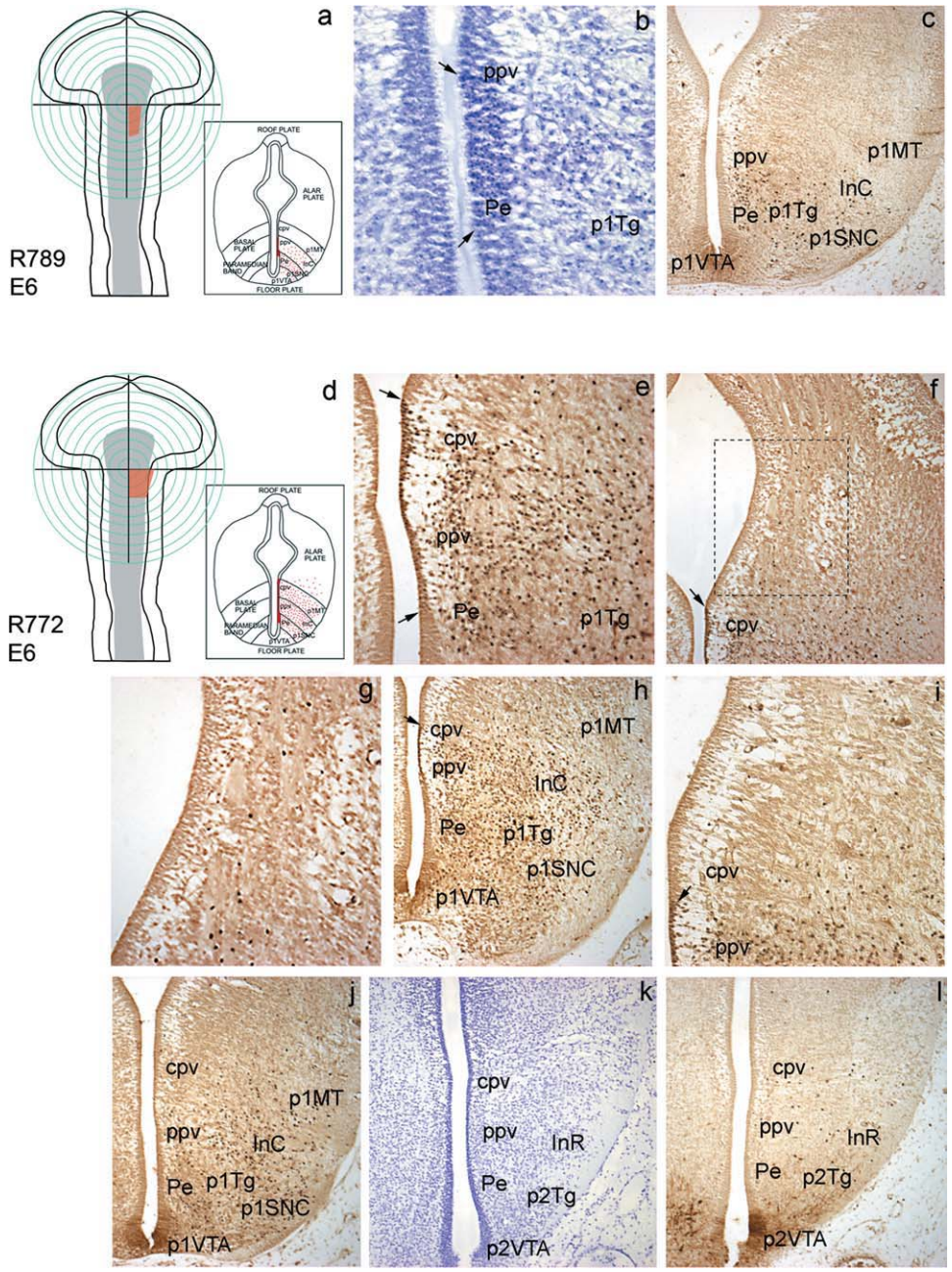

Fig. 3. Homotopic and homochronic chimeras of the p1 basal plate (Table 2). (**a–l**) Basal band grafts (a–c) and basal/parabasal band grafts (d–l). (a, d) Drawings depicting a coronal section of the chick neural tube and the location and size of the quail graft. (b) High-powered image from a coronal section of a basal plate graft at HH29 stained with Nissl's, where the ventrodorsal extension of the grafted territory can be seen entering the basal-plate ventricular epithelium (between the arrows). This area corresponds to the orange-colored domain illustrated in the box image of (a). (c) Parallel section immunostained with QCPN. (e–l) A series of coronal sections from case R772, a basal and parabasal graft, immunostained with the QCPN. The sections proceed from posterior to anterior. (e) Low-magnification picture where the size of graft was evaluated by extent of QCPN+ cells in the ventricular layer. (f–i) At E6 (HH29), the quail cells derived from the p1 QCPN+ ventricular site migrated tangentially toward dorsal areas of the p1 prosomere. (j–l) At this stage, we observed quail cells derived from the p1 QCPN+ ventricular site migrating tangentially into p2Tg and InR at the basal plate of p2. For abbreviations, see abbreviation list. [Color figure can be viewed in the online issue, which is available at www.interscience.wiley.com.]

Tangential Migration in the Embryonic Diencephalon

We created a series of ventral diencephalon chimeras and examined long-term graft derivatives (n = 19). In the p1 basal-plate grafts, as opposed to p2, we detected cells tangentially migrating to neighboring dorsal territories. Previous reports have shown that the anterior diencephalic tegmentum (basal p3 or retromammillar tegmentum), together with the hypothalamic mammillar region, originate a migratory cellular stream that contribute to different GABAergic-cell populations, including the subtha-

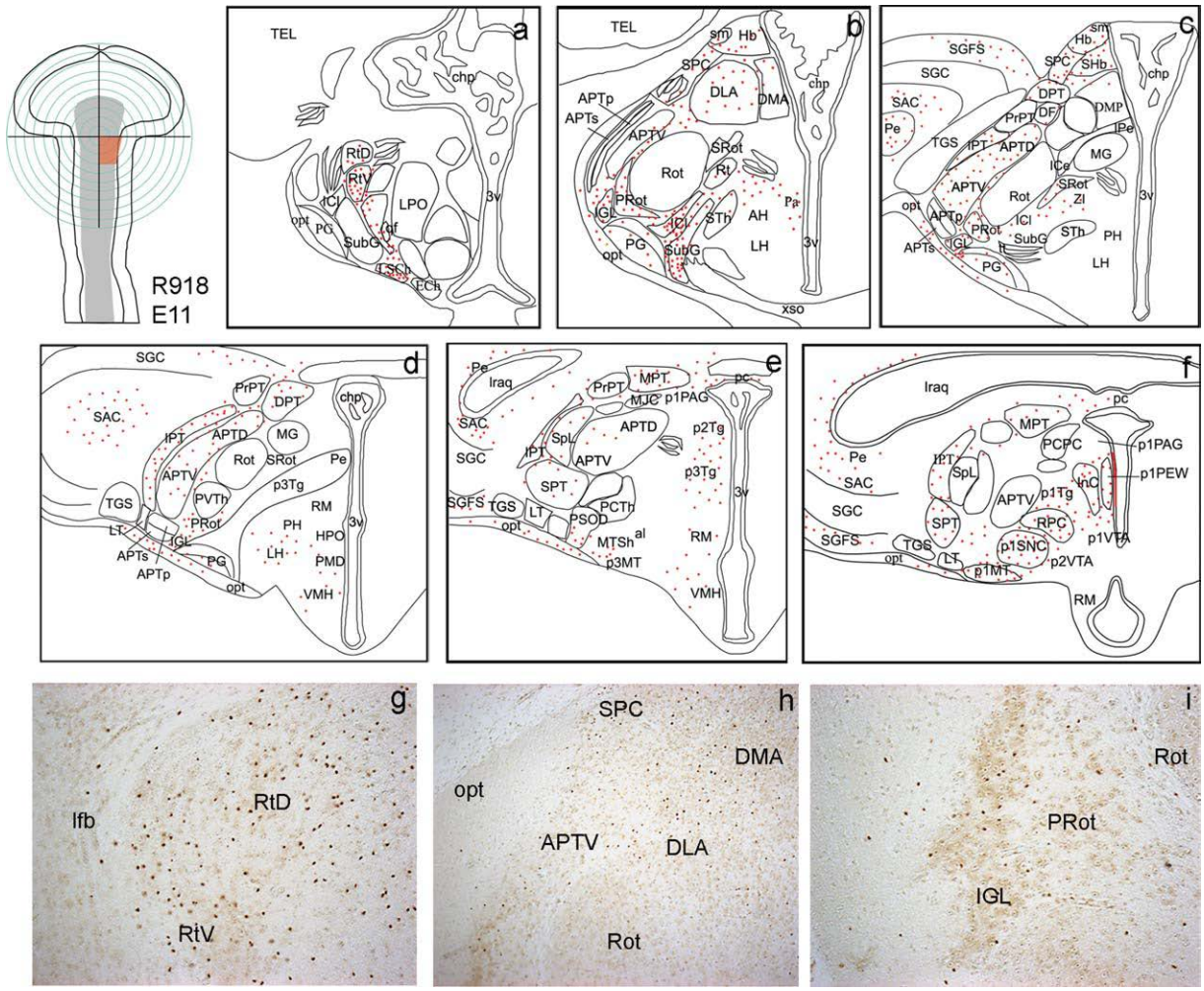

Fig. 4. Mapping cell migration in basal and parabasal grafts of p1 basal plate at HH37 (E11; case R918; Table 3). The drawing in the top left corner depicts the size and locations of the quail graft. (**a–f**) Migrating quail cells from the graft are plotted in red on a drawing of a HH37 embryonic chick brain. Sections are shown from anterior (a) to posterior (f). The quail-derived cells were mapped both in the ventricular neuroepithelium (red areas) and in the mantle zone (red dots). (**g–i**) Coronary sections from case R918 immunostained with QCPN showing quail cells as dark brawn dots. Scattered quail cells can be detected in the neuropiles of the prethalamic (g) and thalamic (h, j) nuclei. Migrating cells were mainly located in the limiting nuclei between the thalamus and pretectum (h) as well as in the superficial thalamic structures (i). No grafted cells were detected in the central nuclear structures (Rot) (h, j). For abbreviations, see abbreviation list. [Color figure can be viewed in the online issue, which is available at www.interscience.wiley.com.]

TABLE 3. List of Long-Survival Chimeric Embryos Used to Characterize the Phenotype of Migrating Cells from Basal Plate p1

Cases	Graft location	Stage of operation	Stage of fixation	Cytoarchitecture, immunohistochemistry and ISH
R359	BPp1	HH9	HH34	CV, QCPN, Tuj1
R369	BPp1	HH9	HH36	CV, QCPN
R918	BPp1	HH9	HH37	CV, QCPN
R941	BPp1	HH9	HH39	CV, QCPN
R514	BPp1	HH9	HH40	CV, QCPN, PLP
R548	BPp1	HH9	HH40	CV, QCPN, PLP
R563	BPp1	HH9	HH40	CV, QCPN, PLP, MAP2
R565	BPp1	HH9	HH40	CV, QCPN, PLP
R974	BPp1	HH9	HH40	CV, QCPN, *plp/dm20*
R969	BPp1	HH9	HH40	CV, QCPN, *Gad65*

Note. BPp1: basal plate prosomere 1. HH, stages of Hamburger and Hamilton (1951); PLP, rat monoclonal antibody used as oligodendrocyte marker; QCPN, monoclonal antiquail antibody.

lamic nucleus, in chick (García-López et al., 2004), and in mouse embryos (Delaunay et al., 2009; Zhao et al., 2008).

We assessed the relative contribution of each region of the p1 basal plate toward tangential migration, comparing the ventricular distribution of quail cells at stages HH29–30 with the migratory behavior, including specifically different basal plate domains of p1 (n = 9; Table 2). As a result, we discovered that grafts of p1 parame-

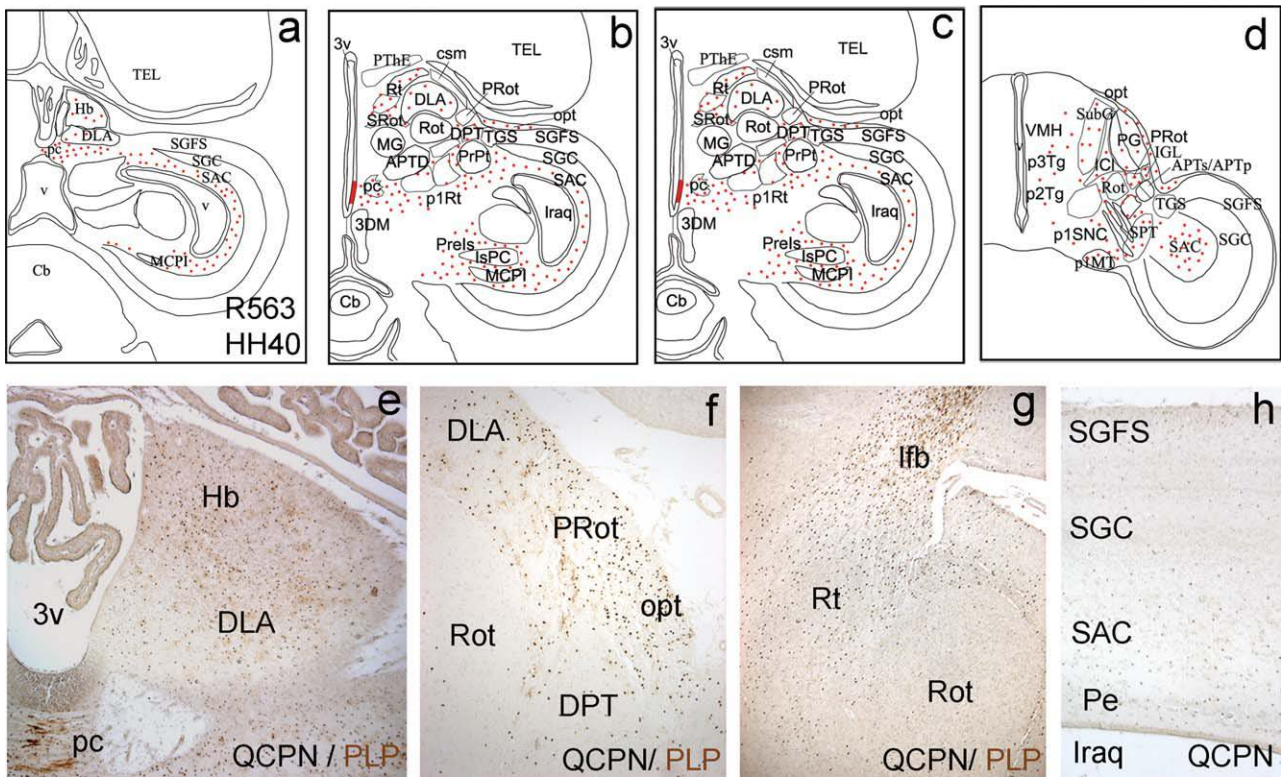

Fig. 5. Mapping cell migration in basal and parabasal band grafts of p1 basal plate at HH40 (E14; case R563; Table 3). **a–d:** Schematic representation of horizontal sections from dorsal (a) to ventral (d). The grafted domain in the ventricular neuroepithelium is colored in red, and the migrating quail cells in the mantle layer are represented by red dots. **e–h:** Horizontal sections where QCPN (black) and PLP (brown) staining was performed to detect quail cells and OPC, respectively. QCPN+ cells were detected in the epithalamus (e), superficial thalamus (f), anterior thalamus, prethalamus, and telencephalic peduncular area (g) and in layers of mesencephalic optic tectum (h). QCPN and PLP positive cells coincide in most of the regions and were more abundant in axonal tracts (opt, lfb). For abbreviations, see abbreviation list. [Color figure can be viewed in the online issue, which is available at www.interscience.wiley.com.]

dian (pm) and basal (b) bands of the basal plate ($n = 5$) did not present tangentially migrating quail cells outside p1 tegmentum (case example: R789; Fig. 3a–c). In these chimeras, quail cells appeared at the periventricular and periventricular plexiforme stratus. Also, we observed quail cells homogenously distributed into basal-plate derivatives, such as the anterior pole of the substantia nigra and interstitial nucleus of Cajal (Fig. 3b,c). In contrast, the grafts that included pb ($n = 4$) presented a significant number of tangentially migrating cells (case example: R772; Fig. 3d–l). In these cases, the quail cells invaded the subventricular (Fig. 3e–g) and mantle zones (Fig. 3h,i). Also, a few cells were detected in the marginal (Fig. 3h,j) zones of p1 alar plate.

The time course, migratory pathways, and allocation of these tangentially migrating quail cells were detected in chimeras analyzed from stage HH25 to HH37 (from 4.5 to 11 days of incubation; $n = 8$). We have previously described that the first tangentially migrating cells were detected in HH25 chimeras. At this stage, quail cells were observed leaving from basal grafts of p1 and invading the adjacent alar plate area, coursing perpendicularly to the radial axis of the neural wall (i.e., moving tangentially) (Fig. 2o). In similar experiments fixed at later stages (HH29–37), this tangential migration of basal cells was observed at more dorsal levels in the developing alar mantle layer (Figs. 3e–l and 4a–i). On the other hand, we observed several quail cells rostrally into the basal plate of p2 at HH29 (Fig. 3k,l), suggesting an additional rostral movement.

The ventrodorsal migrating quail cells progressively dispersed throughout the p1, p2, and p3 alar plates between stages HH29 and HH37. Interestingly, at stages HH34–37 (8–11 days of incubation), migrating quail cells mainly followed the posterior and anterior limits of p1, with mesencephalic and p2 derivatives, respectively (Fig. 4f,h), and even invading the posterior commissure (pc) in the roof plate (Fig. 4f). Indeed, following the limit between p1 and p2, quail cells entered into the habenular region (Hb) (Fig. 4b,c). Throughout the superficial visual nuclei, mainly the intergeniculate leaflet area (IGL), quail cells advanced rostrally into ventral p2 and then moved dorsolaterally into the zona limitans (between p2 and p3) to populate the anterior thalamus (DLA) and reticular nucleus of the prethalamus (Rt) (Fig. 4a,b). In the basal plate, quail cells migrated following the developing medial and lateral forebrain bundle (lfb) toward the telencephalon (Fig. 4). At HH37–40 (11–14 days of incubation), quail cells were more abundant in the alar diencephalic regions: (i) in the pretectum (p1 alar plate): localized in the anterior pretectal nucleus (APT), superficial cell plate of the APT (APTp), subpretectal nucleus (SPT), and intermediate

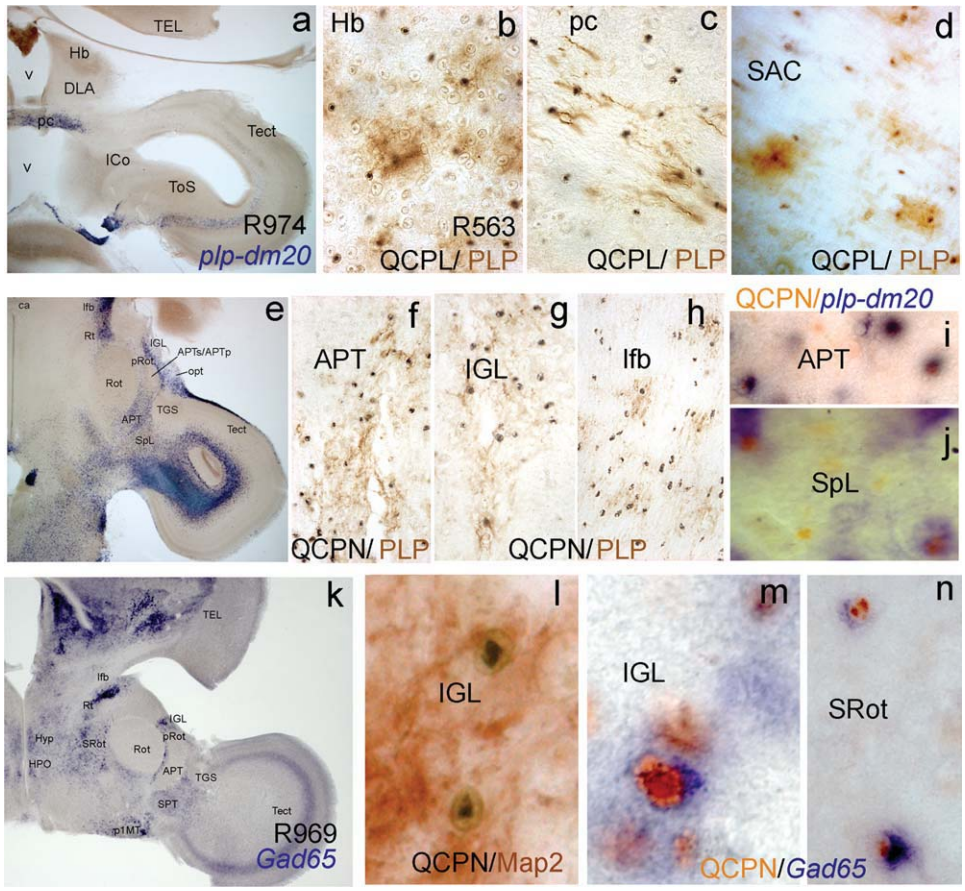

Fig. 6. Phenotype of migrating quail cells. (**a**, **e**) Horizontal sections of R974 chimera where OPC were detected by *plp-dm20* staining. (**b–d**, **f–h**) Close-up images of parallel sections of (a): (b–d) and (e): (f–h) processed by immunohistochemistry showing that the majority of the QCPN+ cells (as detected by nickel-DAB staining: black nucleus) are PLP+ (as seen by normal DAB staining: brown cytoplasm). The areas were identified by the anatomical annotations. (**i, j**) High-powered images of parallel sections from the same chimera, where QCPN+ cells (orange/brown nuclei) expressed *plp/dm20* (in blue). **k–n:** Neuronal phenotype of the tangentially migrating cells in basal plate p1 chimeras at stage HH40. (k) Horizontal section processed by *Gad65* ISH, where the thalamic/pretectal limit (pRot area) and the superficial thalamic nucleus (IGL) can be seen to be populated by *Gad65* expressing cells. (l) R563 chimera stained for QCPN (in black) and the neuronal marker Map2 (in brown). Double-stained cells were observed in the IGL nucleus. (m, n) High-powered image of a parallel section to (k) showing cellular colocalization of *Gad65* (blue) and QCPN (red) in the SRot and IGL neuropiles. For abbreviations, see abbreviation list.

pretectal nucleus (IPT); (ii) in the thalamus, they were present in the IGL and perirotundic area (PRot); (iii) whereas in the prethalamus, we detected graft-derived cells in the subgeniculate nucleus of prethalamus (SubG) as well as in the dorsal (RtD) and ventral (RtV) reticular nucleus (Figs. 4 and 5). At HH40, quail cells were abundant in the Hb (Fig. 5a,e), optic tract (opt), and superficial primary visual nuclei of the diencephalon (Fig. 5b–d,f). Interestingly, quail cells accumulated into the opt and the lfb, invading the telencephalic peduncular area (Fig. 5f,g). Although few quail cells were detected entering the optic tectum at HH37 (Fig. 4c–f), these were more abundant at stage HH40 (Fig. 5a–d,h), and mainly accumulated in the white matter (SAC). Finally, several scattered quail cells were also observed more caudally, in the anterior cerebellar folia (data not shown).

Phenotype of Migrated Cells

P1 parabasal chimeras were analyzed at stages HH40–43 (n = 8; 14–17 days of incubation), by double labeling brain sections with QCPN mAb and PLP mAb, the latter considered to be an OPC marker in birds (Perez-Villegas et al., 1999). The oligodendrocytes derived from the graft were therefore defined as $QCPN^+/PLP^+$ cells. To control the parabasal location of the grafts, we compared the ventricular region of $QCPN^+$ cells with the expression pattern of *Sulf1* at early stages of development (Fig. 2m–p). Then, we confirmed that the grafted quail neuroepithelium corresponded to the prospective territory of p1 parabasal band.

Outside the ventricular neuroepithelium, the oligodendrocyte distribution originating from either the host or the graft epithelium was carefully examined in the alar diencephalic and telencephalic structures (Figs. 5 and 6). Double immunohistochemistry with QCPN-Mab and the OPC marker PLP-Mab demonstrated that the majority of migrated cells were OPC (Fig. 6a–h). Also, we observed OPC/QCPN + in the embryos processed for *in situ* hybridization to detect *plp/dm20* mRNA and immunostaining for the antiquail antibody (Fig. 6a,e,i,j).

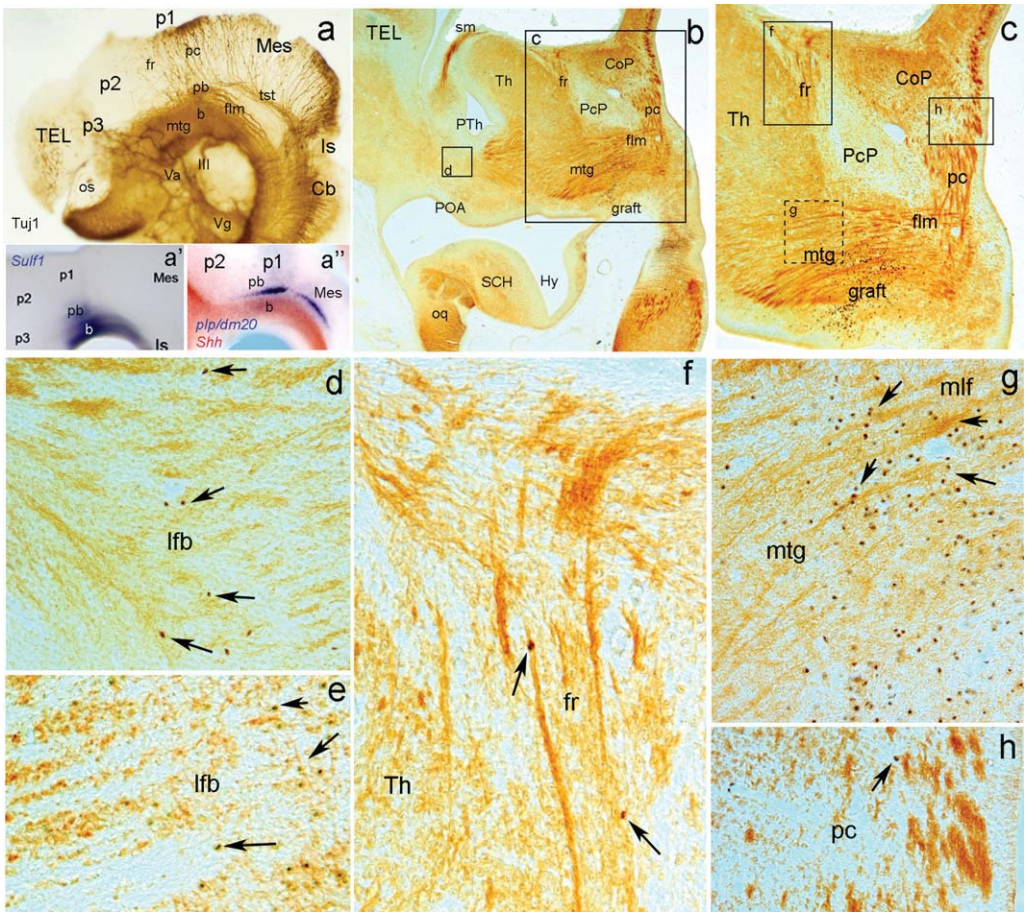

Fig. 7. Tangential migration of parabasal cells in relation to axonal tracts. (**a**) Tuj1 immunostaining in whole-mount chick embryos at stage HH24 showing the distribution of axonal tracts in the brain. (**a, a**′) Images of diencephalic basal plate showing: (a′) *In situ* hybridization of whole-mount chick embryos at stage HH24 for *Sulf1*. (**a**″) Double *in situ* hybridization of whole-mount chick embryos at stage HH25 for *plp/dm20* (blue) and *Shh* (red). (**b–h**) Images from chimera R359 (HH34), stained for QCPN (in black) and Tuj1 (brown) or MAP2 in (e) (brown). (b) Para-sagittal section of the diencephalon. The larger box marks the area shown in (c), whereas the smaller box marks the area shown in (d) and (e). (c) Higher-powered image showing the expression pattern of grafted cells (QCPN+) in the basal and alar plates in relation to the axonal tracts (Tuj1+). As indicated in the boxed areas, these regions correspond to the images shown in (f–h). (d, e) Parallel sections processed by QCPN and Tuj1 (d) or QCPN and MAP2 (e), demonstrating the close relationship between migrating quail cells (arrows) and the axons of the lateral forebrain bundle. (f) QCPN+ positive cells (arrows) detected in contact with retroflexus tract axonal fascicles. (g) QCPN+ positive cells (arrows) in contact with axons of the tegmental longitudinal tracts. (h) QCPN+ positive cells (arrows) in contact with axonal fascicles of the posterior commissure. For abbreviations, see abbreviation list. [Color figure can be viewed in the online issue, which is available at www.interscience.wiley.com.]

Several quail migrating cells (QCPN+) were immunoreactive for the specific neuronal marker Map2 (Fig. 6l), in agreement to our previous results showing that *plp/dm-20* neuroepithelial precursors in mouse embryos generated GABAergic neurons of the diencephalic and hypothalamic nuclei (Delaunay et al., 2009). QCPN staining and *in situ* hybridization for *Gad65* mRNA confirmed the presence of QCPN+/Gad65+ cells in different alar diencephalic areas (Fig. 6k,m,n).

Axonal Tracts and Cell Migration

Cells originating from the parabasal band of p1, where *Sulf1* and *plp-dm20* expression indicates ventricular precursors (Fig. 7a′,a″), migrated tangentially toward the dorsal and rostral mantle layer of other prosomeres, by following specific routes that could be related to the axonal tracts (Fig. 7a).

At the limit between mesencephalon and pretectum, axons of the pc could be the substrate of this migratory stream (Fig. 7a,b). Similar mechanisms could operate at the limit between pretectum and thalamus, where axons of the retroflexus fascicle (fr) could also be the substrate for dorsal migration (Fig. 7a,b). We confirmed the preferential localization of QCPN+ cells in Tuj1+ axonal fascicles in these two tracts at stage HH34 (Fig. 7b,c,f,h). Moreover, cells leaving the basal plate or entering the telencephalic peduncle were also associated to axonal fascicles (Fig. 7g,d,e). At later stages of development, we also detected the accumulation of QCPN+/PLP+ (quail OPC) in the axonal tracts (Fig. 5f,g).

DISCUSSION

The basal-plate neuroepithelium of prosomere 1 (p1) presents special molecular characteristics that could be interpreted as a transitional region between midbrain

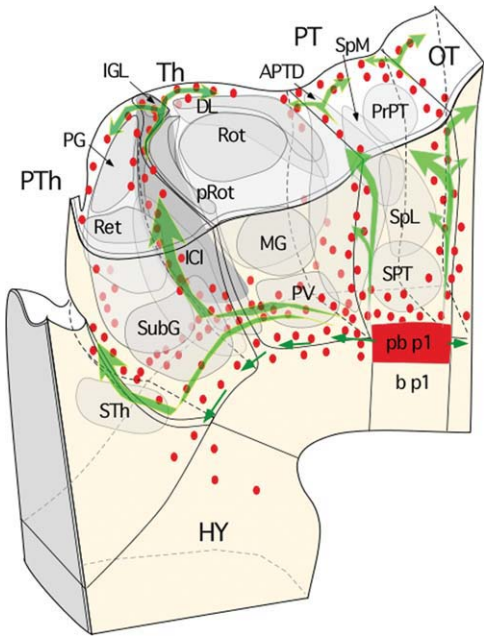

Fig. 8. 3D model representing the migratory routes followed by oligodendrocyte precursors in the developing avian brain. Drawing represents a brain at stage HH35 (E9). The neuroepithelium of p1 parabasal column is colored in red. The arrows indicate the migratory pathways and red dots represent migrating quail cells. Note that oligodendrocyte progenitors from the p1 parabasal column invade diencephalic alar plates as well as more rostral areas including the telencephalic peduncle. Preferential routes follow interprosomeric boundaries in the diencephalon, where early axonal tracts are localized; then from the surface they spread toward the anterior and posterior regions following the optic tract fibers. For abbreviations, see abbreviation list. [Color figure can be viewed in the online issue, which is available at www.interscience.wiley.com.]

and forebrain tegmental regions. Columnar neuroepithelial domains of the rhombencephalic basal plate suffer progressive modifications in mesencephalic and p1 basal plates to establish the molecular complexity that characterizes the thalamic and hypothalamic basal plates (Gimeno and Martinez, 2007). Columnar domains in the mesencephalon and p1 basal plates seem to be induced by Shh signaling (Agarwala and Ragsdale, 2002; Agarwala et al., 2001; Delaunay et al., 2009; Gimeno and Martinez, 2007; Perez-Balaguer et al., 2009; Watanabe and Nakamura, 2000), such as the longitudinal microzonal patterns described in the spinal cord and rhombencephalon (Ericson et al., 1995; Yamada et al., 1991). These molecular domains regulate histogenetic mechanisms that may locally represent the creation of neuroepithelial progenitors with different cellular fates. These newly formed neural cells would then migrate toward the mantle layer and other brain areas. A similar process can be observed in the entopeduncular area and medial ganglionic eminence of the telencephalic subpallium, including the expression of *Shh*, *Sulf1*, and plp/*dm20*. These variations could be interpreted as the transition between diencephalon and telencephalon, where abundant progenitors are specified to develop as OPC and cortical interneurons after extensive migration into the pallium (Cobos et al., 2001; Marín and Rubenstein, 2003; Oliver et al., 2001).

Cells originating in the parabasal band of p1 basal plate migrated tangentially toward dorsal and rostral mantle layers (Fig. 8), following the axonal tracts, which could be the substrate for this migration. It is interesting to note that the p1 parabasal band is a meeting point for multiple axonal tracts. The mantle layer of this region is traversed by the longitudinal fascicles and is where the retroflexus tract and pc fibers meet and change their direction toward caudal regions of the neural tube. In the telencephalon, the peduncular region is also a meeting point where multiple axonal tracts intersect, including the lateral prosencephalic fascicle and the fornix.

The spatial relationship between axonal tract intersections and the expression of OPC genetic markers in the ventricular epithelium suggests the existence of inductive signals from axonal tracts to the epithelial progenitors. Moreover, the dorsal expansion of *Shh* expression in the neuroepithelium of transitional areas between brain regions (the mesencephalic-p1 basal plates and telencephalic entopeduncular area) could imply the activation of *plp/dm-20* and *Sulf1* expression in parabasal domains, where axonal influences could represent an active co-factor and be required for OPC specification and migration. OPC migration in the optic nerve seems to be influenced by *Shh* expression in the preoptic area (Merchán et al., 2007).

Regarding the GABAergic neurons, it is interesting to detect an early expression of *GAD65* in the mantle layer of the migratory routes for p1 cells. Although the interaction of these cells with p1 parabasal migratory neurons needs to be adequately analyzed, the expression of *Fgf19*, *Mash1*, *Pax6*, and *Mgn* could indicate a local GABAergic specification of p1 parabasal progenitors (Gimeno and Martinez, 2007). Similar results have been observed in mouse by clonal analysis experiments using *Olig2* or *plp/dm-20* as a reporter genes (Delaunay et al., 2009; Ono et al., 2008).

ACKNOWLEDGMENTS

We thank our laboratory technicians M. Ródenas, C. Redondo, A. Torregrosa, and O. Bahamonde for their technical assistance in this study; and Dr. Jones Barbera for the English correction.

REFERENCES

Agarwala S, Ragsdale CW. 2002. A role for midbrain arcs in nucleogenesis. Development 129:5779–5788.

Agarwala S, Sanders TA, Ragsdale CW. 2001. Sonic hedgehog control of size and shape in midbrain pattern formation. Science 291:2147–2150.

Alvarado-Mallart RM, Sotelo C. 1984. Homotopic and heterotopic transplantation of quail tectal primordial in chick embryos: Organization of the retino-tectal projections in the chimeric embryos. Dev Biol 103:378–398.

Asou H, Hamada K, Miyazaki T, Hayashi K, Takeda Y, Marret S, Delpech B, Itoh K, Uyemura K. 1995. CNS myelinogenesis in vitro: Time course and pattern of rat oligodendrocyte development. J Neurosci Res 40:519–534.

Braquart-Varnier C, Danesin C, Clouscard-Martinato C, Agius E, Escalas N, Benazeraf B, Ai X, Emerson C, Cochard P, Soula C. 2004. A subtractive approach to characterize genes with regionalized expression in the gliogenic ventral neuroepithelium: Identification of chick *Sulfatase* 1 as a new oligodendrocyte lineage gene. Mol Cell Neurosci 25:612–628.

Cobos I, Puelles L, Martínez S. 2001. The avian telencephalic subpallium originates inhibitory neurons that invade tangentially the pallium (dorsal ventricular ridge and cortical areas). Dev Biol 239:30–45.

Cochard P, Giess MC. 1995. Oligodendrocyte lineage. C.R. Seances Soc Biol Fil 189:263–269.
Delaunay D, Heydon K, Cumano A, Schwab MH, Thomas JL, Suter U, Nave KA, Zalc B, Spassky N. 2008. Early neuronal and glial fate restriction of embryonic neural stem cells. J Neurosci 28:2551–2562.
Delaunay D, Heydon K, Miguez A, Schwab M, Nave KA, Thomas JL, Spassky N, Martinez S, Zalc B. 2009. Genetic tracing of subpopulation neurons in the prethalamus of mice (*Mus musculus*). J Comp Neurol 512:74–83.
Dickinson PJ, Fanarraga ML, Griffiths IR, Barrie JM, Kyriakides E, Montague P. 1996. Oligodendrocyte progenitors in the embryonic spinal cord express DM-20. Neuropathol Appl Neurobiol 22:188–198.
Echevarría D, Vieira C, Martínez S. 2001. Mammalian neural tube grafting experiments: An in vitro system for mouse experimental embryology. Int J Dev Biol 45:895–902.
Ericson J, Muhr J, Jessell TM, Edlund T. 1995. Sonic hedgehog: A common signal for ventral patterning along the rostrocaudal axis of the neural tube. Int J Dev Biol 39:809–816 (Review).
García-López R, Soula C, Martinez S. 2009. Expression analysis of Sulf1 in the chick forebrain at early and late stages of development. Dev Dyn 238:2418–2429.
García-López R, Vieira C, Echevarria D, Martinez S. 2004. Fate map of the diencephalon and the zona limitans at the 10-somites stage in chick embryos. Dev Biol 268:514–530.
Gimeno L, Martinez S. 2007. Expression of chick Fgf19 and mouse Fgf15 orthologs is regulated in the developing brain by Fgf8 and Shh. Dev Dyn 236:2285–2297.
Griffiths I, Klugmann M, Anderson T, Thomson C, Vouyiouklis D, Nave KA. 1998. Current concepts of PLP, its role in the nervous system. Microsc Res Tech 41:344–358.
Hall H, Giese NA, Richardson WD. 1996. Spinal cord oligodendrocytes develop from ventrally derived progenitor cells that express PDGFα receptors. Development 122:4085–4094.
Hamburger V, Hamilton HL. 1951. A series of normal stages in the development of the chick embryo. J Morphol 88:49–92.
Henrique D, Adam J, Myat A, Chitnis A, Lewis J, Ish-Horowicz D. 1995. Expression of a Delta homologue in prospective neurons in the chick. Nature 375:787–790.
Kettenmann H, Ransom BR. 1995. "Neuroglia". New York: Oxford University Press.
Kitagawa K, Sinoway MP, Yang C, Gould RM, Colman DR. 1993. A proteolipid protein gene family: Expression in sharks and rays and possible evolution from a ancestral gene encoding a pore-forming polypeptide. Neuron 11:433–448.
Leber SM, Sanes JR. 1995. Migratory paths of neurons and glia in the embryonic chick spinal cord. Neuroscience 15:1236–1248.
Leber SM, Yamagata M, Sanes JR. 1996. Gene transfer using replication-defective retroviral and adenoviral vectors. Methods Cell Biol 51:161–183.
LeDouarin NM. 1969. Particularités du noyan interphasique chez la caille japonaise (Coturnix coturnix japonica). Utilisation de ces particularités comme "marquage biologique" dans les recherchers sur les interactions tissulaires et les migrations cellulaires au cours de l'ontogénèse. Bull Soc Fr Belg 103:435–452.
LeDouarin NM. 1993. Embryonic neural chimaeras in the study of brain development. Trends Neurosci 16:64–72.
Less MB, Brostoff SW. 1984. Proteins of myelin. In: Morell P, editor. Myelin. New York: Plenum. pp.197–224.
Marín O, Rubenstein JL. 2003. Cell migration in the forebrain. Annu Rev Neurosci 26:441–83 (Review).
Merchán P, Bribián A, Sánchez-Camacho C, Lezameta M, Bovolenta P, de Castro F. 2007. Sonic hedgehog promotes the migration and proliferation of optic nerve oligodendrocyte precursors. Mol Cell Neurosci 36:355–368.
Miller RH, Ono K. 1998. Morphological analysis of the early stages of oligodendrocyte development in the vertebrate central nervous system. Microsc Res Tech 41:441–453.
Nishiyama A, Lin XH, Giese N, Heldin CH, Stallcup WB. 1996. Co-localization of NG2 proteoglycan and PDGF alpha receptor on O2A progenitor cells in the developing rat brain. J Neurosci Res 43:299–314.
Noble M, Murray K, Stroobant P, Waterfield MD, Riddle P. 1988. Platelet-derived growth factor promotes division and motility and inhibits premature differentiation of the oligodendrocyte/type-2 astrocyte progenitor cell. Nature 333:560–562.
Noll E, Miller RH. 1993. Oligodendrocyte precursors originate at the ventral ventricular zone dorsal to the ventral midline region in the embryonic rat spinal cord. Development 118:563–573.
Olivier C, Cobos I, Perez-Villegas EM, Spassky N, Zalc B, Martinez S, Thomas JL. 2001. Monofocal origin of telencephalic oligodendrocytes in the anterior entopeduncular area of the chick embryo. Development 128:1757–1769.
Ono K, Rashmi B, Payne J, Rutishauser U, Miller RH. 1995. Early development and dispersal of oligodendrocyte precursors in the embryonic chick spinal cord. Development 121:1743–1754.
Ono K, Takebayashi H, Ikeda K, Furusho M, Nishizawa T, Watanabe K, Ikenaka K. 2008. Spatio-temporal changes in the differentiation of Olig2 progenitors in the forebrain, and the impact on astrocyte development in the dorsal pallium. Dev Biol 320:456–468.
Ono K, Takebayashi H, Ikenaka K. 2009. Olig2 transcription factor in the developing and injured brain; cell lineage and glial development. Mol Cell 27:397–401.
Ono K, Yasui Y, Rutishauser U, Miller RH. 1997. Focal ventricular origin and migration of oligodendrocyte precursors into the chick optic nerve. Neuron 19:283–292.
Orentas DM, Miller RH. 1996. The origin of spinal cord oligodendrocytes is dependent on local influences from the notochord. Dev Biol 177:43–33.
Perez-Balaguer A, Puelles E, Wurst W, Martinez S. 2009. Shh dependent and independent maintenance of basal midbrain. Mech Dev 126:301–313.
Perez-Villegas EM, Olivier C, Spassky N, Poncet C, Cohard P, Zalc B, Thomas JL, Martinez S. 1999. Early specification of oligodendrocytes in the chick embryonic brain. Dev Biol 216:98–113.
Popot JL, Dinh DP, Dautigny A. 1991. Major myelin proteolipid the 4-α-helix topology. J Membr Biol 120:233–246.
Pringle NP, Guthrie S, Lumsden A, Richardson WD. 1992. PDGF receptors in the rat CNS: During late neurogenesis, PDGF α-receptor expression appears to be restricted to glial cells of the oligodendrocyte lineage. Development 115:535–551.
Pringle NP, Richardson W. 1993. A singularity of PDGF α-receptor expression in the dorsoventral axis of the neural tube may define the origin of the oligodendrocyte lineage. Development 117:525–533.
Pringle NP, Yu W, Guthrie S, Roelink H, Lumsden A, Peterson A. 1996. Determination of neuroepithelial cells fate: Induction of the oligodendrocyte lineage by ventral midline cells and Sonic hedgehog. Dev Biol 177:30–42.
Puelles L, Martinez de-la-Torre M, Paxinos G, Watson Ch, Martinez S. 2007 The chick brain in stereotaxic coordinates: An atlas featuring neuromeric subdivisions and mammalian homologies. New York: Academic Press.
Puelles L, Rubenstein JL. 2003. Forebrain gene expression domains and the evolving prosomeric model. Trends Neurosci 26:469–476.
Richardson WD, Pringle NP, Yu WP, Hall AC. 1997. Origins of spinal cord oligodendrocytes: Possible developmental and evolutionary relationships with motor neurons. Dev Neurosci 19:58–68.
Small RK, Riddle P, Noble M. 1987. Evidence for migration of oligodendrocyte-type-2 astrocyte progenitor cells into the developing rat optic nerve. Nature 328:155–157.
Soriano P. 1997. The PDGF α receptor is required for neural crest cell development and for normal patterning of the somites. Development 124:2691–2700.
Spassky N, Goujet-Zalc C, Parmantier E, Olivier C, Martinez S, Ivanova A, Ikenaka K, Macklin W, Cerruti I, Zalc B, Thomas JL. 1998. Multiple restricted origin of oligodendrocytes. J Neurosci 18:8331–8343.
Spassky N, Olivier C, Perez-Villegas E, Goujet-Zalc C, Martínez S, Thomas Jl, Zalc B. 2000. Single or multiple oligodendroglial lineages: A controversy. Glia 29:143–148.
Timsit S, Martinez S, Allinquant B, Peyron F, Puelles L, Zalc B. 1995. Oligodendrocytes originate in a restricted zone of the embryonic ventral neural tube define by DM-20 mRNA expression. J Neurosci 15:1012–1024.
Timsit SG, Ballycuif L, Colman D, Zalc B. 1992. DM20 messenger RNA is expressed during the embryonic development of the nervous system of the mouse. J Neurochem 58:1172–1175.
Wahle S, Stoffel W. 1998. Cotranslational integration of myelin protein (PLP) into the membrane of endoplasmic reticulum: Analysis of topology by glycosylation scanning and protease domain protection assay. Glia 24:226–235.
Warf BC, Fok-Seang J, Miller RH. 1991. Evidence for the ventral origin of oligodendrocyte precursors in the rat spinal cord. J Neurosci 11:2477–2488.
Watanabe Y, Nakamura H. 2000. Control of chick tectum territory along dorsoventral axis by Sonic hedgehog. Development 127:1131–1140.
Yamada T, Placzek M, Tanaka H, Dodd J, Jessell TM. 1991. Control of cell pattern in the developing nervous system: Polarizing activity of the floor plate and notochord. Cell 64:635–647.
Yan Y, Lagenaur C, Narayanan V. 1993. Molecular cloning of M6: Identification of a PLP/DM-20 gene family. Neuron 11:423–431.
Yu WP, Collarini EJ, Pringle NP, Richardson WD. 1994. Embryonic expression of myelin genes: Evidence for a focal source of oligodendrocyte precursors in the ventricular zone of the neural tube. Neuron 12:1353–1362.
Zhao GY, Li ZY, Zou HL, Hu ZL, Song NN, Zheng MH, Su CJ, Ding YQ. 2008. Expression of the transcription factor GATA3 in the postnatal mouse central nervous system. Neurosci Res 61:420–428.